Comparative RNA-sequencing profiled the differential gene expression of liver in response to acetyl-CoA carboxylase inhibitor GS-0976 in a mouse model of NASH

Ying Lu[1,2,*], Xiaolan Su[1,2,*], Manyu Zhao[2], Qianru Zhang[2,3], Chuang Liu[1,2], Qinhuai Lai[1,2], Sijia Wu[2], Aiping Fang[1,2], Jinliang Yang[1,2,3], Xiaoxin Chen[3] and Yuqin Yao[2]

[1] State Key Laboratory of Biotherapy and Cancer Center, West China Hospital and Healthy Food Evaluation Research Center, Sichuan University, Chengdu, China

[2] West China School of Public Health and West China Fourth Hospital, Healthy Food Evaluation Research Center, Sichuan University, Chengdu, China

[3] Guangdong Zhongsheng Pharmaceutical Co., Ltd., Dongguan, China

[*] These authors contributed equally to this work.

ABSTRACT

Background. Non-alcoholic steatohepatitis (NASH) is a progressive liver disease characterized by hepatic steatosis, lobular inflammation and fibrosis. Acetyl-CoA carboxylase (ACC) isoform 1 and 2 involved in de novo lipogenesis (DNL) and fatty acid oxidation have been identified as a therapeutic target in NASH. GS-0976, the inhibitor of ACC1 and ACC2, has achieved favorable therapeutic effects in clinical trials with NASH. The purpose of this study was to explore the transcriptional alterations regulated by GS-0976 in NASH.

Methods. C57BL/6 mice were fed on a choline-deficient, L-amino acid-defined, high-fat diet (CDAHFD) or normal diet for 12 weeks. Mice were treated with or without GS-0976 (3 mg/kg per day) in the last 8 weeks. Oil Red O, Haematoxylin-eosin (H & E), and Sirius Red were used to evaluate hepatic steatosis, inflammation and fibrosis. The comparative RNA-sequencing was conducted to analyse the hepatic gene expression profiles in mice. Reverse transcription–polymerase chain reaction analysis was performed to validate the differential expression of representative genes.

Results. GS-0976 attenuated the steatosis, inflammation, and fibrosis of NASH in CDAHFD mouse model. High-throughput sequencing and differential gene expression analysis showed that there were 516 up-regulated genes and 525 down-regulated genes after GS-0976 treatment. Genes involved in the metabolic process, extracellular matrix formation, immune response, and angiogenesis were significantly enriched. The "Metabolic pathways" and "ECM-receptor interaction" pathways were the most significantly enriched KEGG pathways in the up-regulated and down-regulated differentially expressed genes (DEGs), respectively.

Conclusions. Transcriptome analysis showed that GS-0976 could regulate the expression of genes related to metabolism, inflammation and fibrosis in NASH. The global transcriptomic changes in gene expression promote the further understanding for the inhibition mechanisms of GS-0976 in NASH.

Submitted 16 August 2019
Accepted 28 October 2019
Published 20 December 2019

Corresponding authors
Yuqin Yao, yuqin_yao@scu.edu.cn
Xiaoxin Chen, chenzhenyu2000@zspcl.com

Academic editor
Xiang-Jiao Yang

Additional Information and Declarations can be found on page 14

DOI **10.7717/peerj.8115**

How to cite this article Lu Y, Su X, Zhao M, Zhang Q, Liu C, Lai Q, Wu S, Fang A, Yang J, Chen X, Yao Y. 2019. Comparative RNA-sequencing profiled the differential gene expression of liver in response to acetyl-CoA carboxylase inhibitor GS-0976 in a mouse model of NASH. *PeerJ* **7**:e8115 http://doi.org/10.7717/peerj.8115

Subjects Bioinformatics, Molecular Biology, Metabolic Sciences
Keywords Transcriptome, RNA-Seq, Non-alcoholic steatohepatitis, Acetyl-CoA carboxylase inhibitor

INTRODUCTION

Non-alcoholic fatty liver disease (NAFLD) has become one of the most common chronic liver disease (CLD) related to metabolic syndrome, obesity and type 2 diabetes. NAFLD has caused great social and economic burden in the world (*Younossi et al., 2018a*). As a portion of the NAFLD spectrum, NASH is a progressive process characterized by steatohepatitis, lobular inflammation and fibrosis (*Bedossa, 2017*). In the United States, the number of patients with NASH is expected to increase from 16.52 million in 2015 to 27.00 million in 2030 (*Estes et al., 2018*). Lifestyle interventions are considered an effective therapy for NASH, but hard to maintain (*Younossi et al., 2018b*). However, there is no approved pharmacotherapy for NASH.

Disorders of fatty acid metabolism, including increased fatty acid synthesis or DNL, decreased fatty acid oxidation and imbalanced of adipokines, are key factors in the etiology of NASH (*Chalasani et al., 2018*). The DNL plays an important role in fatty acid synthesis and catabolism. Acetyl-CoA carboxylase (ACC) is the first committed and rate-limiting enzyme regulating DNL pathway, which catalyzes the carboxylation of acetyl-CoA into malonyl-CoA. There are two isoforms of ACC in mammals, ACC1 and ACC2, with different distribution in cells and physiological function (*Neuschwander-Tetri, 2010*). ACC1, a cytosolic enzyme, promotes the synthesis of cytosolic malonyl-CoA and is the primary substrate for fatty acid synthesis and elongation. ACC2 is distributed in mitochondrial membrane and generates malonyl coenzyme A. And malonyl coenzyme A inhibits carnitine palmitoyl transferase (CPT-1) by isomerization, thus inhibiting the carrier protein of fatty acids from entering mitochondria for β-oxidation (*Abu-Elheiga et al., 1995*).

Studies have shown that inhibition of ACC expression in liver by knocking out ACC genes or small molecule drugs can significantly reduce the concentration of hepatic triglyceride (TG) and DNL. (*Harriman et al., 2016*; *Harwood Jr et al., 2003*; *Mao et al., 2006*). GS-0976 is one of the effective ACC1 and ACC2 inhibitors for the treatment of NASH. In the obesity rodent model and NASH patients, GS-0976 has a good effect on hepatic steatosis and fibrosis (*Harriman et al., 2016*; *Lawitz et al., 2018*; *Loomba et al., 2018*). These evidences strongly support the view that the inhibition of ACC is an important therapeutic target in NASH. However, little is known about the whole transcriptome regulation with ACC inhibition by GS-0976 treatment. In the present study, to further understand the mechanisms of GS-0976 in NASH, RNA-Seq was used to investigate hepatic gene expression profiles in CDAHFD-induced NASH model. Functional enrichment analysis of the DEGs revealed the potential molecular mechanism of GS-0976 on metabolism, inflammation, fibrosis, and angiogenesis.

MATERIAL AND METHODS

Animals and diets

Male C57BL/6 mice (4 weeks old) were purchased from the Vital-River Animal Ltd (Beijing, China). Animals were housed in a specific pathogen-free environment and maintained on standard diet at a temperature of 24 ± 1 °C and 12/12 h light/dark cycles, with free access to food and water (*Zhang et al., 2017*). The animal procedures were performed in accordance with the standard guidelines and were approved by the institutional animal care and treatment committee of West China Hospital, Sichuan University (Chengdu, China; approval no.182). Mice were divided into three groups at 9 weeks of age and fed with CDAHFD (Research Diets Inc, New Brunswick, New Jersey, USA, A06071302) or normal diet (DASHOU, Chengdu, China) for 4 weeks, respectively. Subsequently, GS-0976 or equal volume of vehicle were given by oral gavage once daily for another 8 weeks. Mice in the GS-0976 group were fed on CDAHFD and GS-0976 (3 mg/kg/d) (*Harriman et al., 2016*). Mice in the Model group and Control group were fed on CDAHFD and vehicle or normal diet, respectively. GS-0976 for clinical trials was purchased from MedchemExpress (Cat.No. HY-16901). The vehicle was made up of 1% carboxymethylcellulose sodium and 0.1% tween 80 with boiling water. GS-0976 was then co-grinded with pre-cooled vehicle and stored at 4 °C. GS-0976 mixture was prepared once a week and was vortexed before administration. Animals were anesthetized with pentobarbital sodium. The terminal blood samples were collected from the eyelids for plasma biochemistry. Liver tissues of all the mice were collected and stored at −80 °C.

Histopathological and biochemical assessment

Fresh liver tissues were fixed in 10% neutral formalin, embedded in paraffin, and cut into 5 μm sections. Sections of formalin-fixed livers were used for H&E, Oil red O staining and Sirius Red staining. The stained slices were observed using BA400 Digital microscope (Motic China Group Co., Ltd). The percent of fibrosis areas were calculated by NanoZoomer Digital Pathology S210. Histological steatosis, inflammation, and ballooning were graded in a blinded manner by an experienced pathologist according to the scoring method described by *Kleiner et al. (2005)*. The NAS scores of steatosis, inflammation and ballooning scores were evaluated.

Blood samples obtained from eyelids were used for evaluating the concentration of serum alanine aminotransferase (ALT), aspartate aminotransferase (AST), high-density lipoprotein (HDL) and low-density lipoprotein (LDL) by a chemistry analyzer (Hitachi 7020, Tokyo, Japan) according to the manufacturer's instructions.

Sample preparation, library construction and RNA-Seq

Total liver RNA from the three mice of each group was extracted using Tiangen RNA prep Pure Plant Kit (Tiangen, Beijing, China). The quantity and quality of the extracted RNA were verified by Qubit®RNA Assay Kit in Qubit® 2.0 Fluorometer (Life Technologies, CA, USA) and the RNA Nano 6000 Assay Kit of the Bioanalyzer 2100 system (Agilent Technologies, CA, USA). The cDNA library construction and sequencing were performed as described before (*Chen et al., 2018*).

Data processing, assembly, and annotation

The acquired data were processed as previously described (*Chen et al., 2018*). Briefly, raw data were first processed through Perl scripts to obtain clean data by removing reads containing adapter, ploy-N and with low quality. Meanwhile, Q20, Q30 and GC content of the clean data were calculated to meet the standard (Q20>90, Q30>85). All the downstream analyses were based on clean data with high quality. Indexes of the reference genome were built using Bowtie v2.0.6 and paired-end clean reads were aligned to the reference genome using TopHat v2.0.9. HTSeq v0.6.1 was used to count the read numbers mapped of each gene. And then RPKM of each gene was calculated based on the length of the gene and reads count mapped to this gene.

Gene expression pattern analysis

Differential expression analysis between two groups was performed using the DESeq R package (1.10.1). DESeq provides statistical routines for determining differential expression in digital gene expression data using a model based on the negative binomial distribution. The results of *P*-values were adjusted using the Benjamini and Hochberg's approach for controlling the False Discovery Rate (FDR). Genes with an adjusted $P < 0.05$ were assigned as differentially expressed.

The identified DEGs were used for bioinformatics analyses. The Gene ontology (GO) analysis were performed using the GOseq R package and was mapped in the GO database (*P*-value ≤ 0.05). The Kyoto Encyclopedia of Genes and Genomes (KEGG) pathway enrichment analysis of the DEGs was conducted using KOBAS software.

Cell culture

The immortalized human hepatic stellate cell line LX-2 (Procell, Wuhan, China) was cultured in DMEM-high glucose supplemented with 20% fetal bovine serum, 100 U/mL penicillin and 100 μg/mL streptomycin. The normal human hepatocyte cell line LO2 were obtained from the Chinese Academy of Sciences (Shanghai, China) and cultured in RPMI-1640 supplemented with 10% fetal bovine serum, 100 U/mL penicillin and 100 μg/mL streptomycin. Cells were maintained at 37 °C in a humidified atmosphere of 5% CO_2 (*Lai et al., 2018*).

Cell treatment

To induce the hepatocyte steatosis in vitro, a mixture of free fatty acids (FFA) comprised by palmitic and oleate at a ratio of 1:2 were supplied in culture medium at the final concentration of 0.8 mM. LO2 cells were seeded on a cover slide in 24-well plates at a density of 10,000 cells per well. After reaching 75–80% confluence, cells were exposed to the indicated concentrations of GS-0976 in the presence of FFA for 24 h. Specifically, LO2 cells with only 0.8 mM FFA treatment were defined as Model group and cells treated without FFA were Control group. To study the effects of GS-0976 on fibrosis, LX-2 cells were administrated with GS-0976 and TGF-β1 (10 ng/mL, Novoprotein, Chain) for 24 h. The mRNA expression of α-smooth muscle actin (α-SMA), type I collagen (COL1A1, COL1A2), type III collagen (COL3A1), connective tissue growth factor (CTGF), Extracellular sulfatase (SULF-2) were evaluated.

Oil Red O staining

After treatment and washes, LO2 cells were fixed in 4% paraformaldehyde for 10 mins, followed by three times washes with PBS, then stained with freshly prepared Oil Red O working solution for 10 mins at room temperature. Cells were then rinsed in 60% isopropanol for 10 s, followed by PBS washing and Hematoxylin stain for 10 mins. Lipid droplets were captured at ×400 magnification using a light microscope (Olympus-CX31, Japan).

RNA isolation and quantitative real-time PCR

Total RNA of LX-2 cells was extracted using cell RNA isolation kit (Foregene, China). First strand cDNA was synthesized by HiScript® II Reverse Transcriptase (Vazyme, China) from 1 μg of total RNA template according to the manufacturer's instruction. Gene expression was quantified by real-time PCR with SYBR Green master mix (Vazyme, China) and CFX96 real-time PCR system (Bio-Rad, USA). The sequence-specific primers of the target gene are given in Table S1. All the experiments were carried out three times and *β-actin* was used as the housekeeping gene. The relative mRNA fold changes were calculated using the $2^{-\Delta\Delta CT}$ method.

Statistical analysis

Statistics were analysed with SPSS 25.0 (IBM Corp., Armonk, NY, USA). One-way ANOVA followed by LSD test was used to assess statistical significance. The data were presented as the mean ± Standard Error of Mean (SEM). P values <0.05 were considered to be significant in this study.

RESULTS

Validation of CDAHFD-induced NASH model in C57BL/6 mice

C57BL/6 mice were maintained on CDAHFD or normal diet for 4 weeks and were co-administered with GS-0976 (3 mg/kg/d) or vehicle for the following eight weeks. The body weight gain and food intake of mice in the Model group were lower than that of mice in the Control group (Figs. 1A, 1B). The liver weight and liver/body weight ratio were increased in the Model group (Figs. 1C, 1D). At the end of 12 weeks, compared with the Control group, the levels of ALT and AST in the model group increased 7.1 times and 3.3 times respectively (Figs. 1E, 1F). Moreover, both the serum high-density lipoprotein (HDL) and low-density lipoprotein (LDL) were decreased in the CDAHFD model compared to the Control group (Figs. 1G, 1H). H&E results showed that there were excessive accumulation of lipid droplets, moderate inflammatory foci and few ballooning cells in the Model group (Figs. 2A–2D). Compared with the Control group, Sirius Red and Oil Red O results showed an increase of fibrosis area and lipid accumulation in the Model group, respectively (Figs. 2G–2J, 2M, 2N). The average NAS score was 6.0 ± 0.0 in CDAHFD fed mice (Fig. 2S). Hence, these results confirmed CDAHFD-induced NASH model was well-established.

GS-0976 treatment inhibited CDAHFD induced NASH development

There was no significant difference in body weight gain and food intake between GS-0976 group and Model group (Figs. 1A, 1B). Notably, the increase in liver weight was inhibited

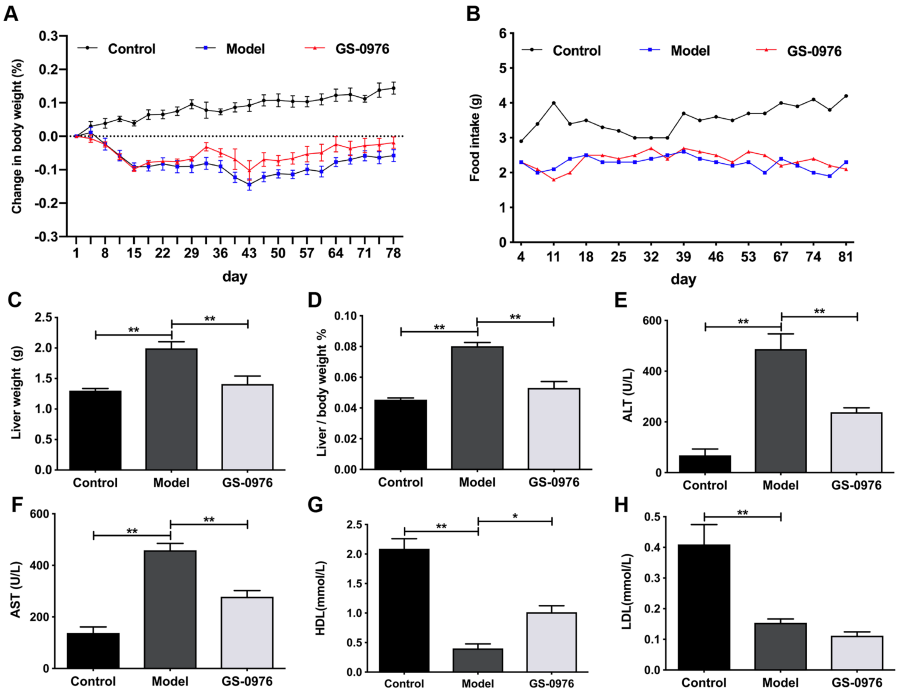

Figure 1 GS-0976 administration attenuated CDAHFD-induced liver injury. Mice were divided into three groups ($n = 5$) and placed either on CDAHFD or normal chow. GS-0976 were given orally 3 mg/kg per day for 8 weeks. (A) Change in body weight, (B) food intake, (C) liver weight, (D) ratio of liver/body weight. (E) Serum levels of ALT, (F) AST , (G) HDL, (H) LDL. Data are shown as means ±SEM. $^{*}P < 0.05$, $^{**}P < 0.001$ compared with the Model group by one-way ANOVA with LSD test.

Full-size DOI: 10.7717/peerj.8115/fig-1

by GS-0976 treatment (Figs. 1C, 1D). The concentration of serum ALT (48.9%), AST (60.7%) was lower in the GS-0976 group than that of the Model group (Figs. 1E, 1F). The Serum HDL was increased 2.54 times and LDL decreased slightly after GS-0976 treatment compared with Model group (Figs. 1G, 1H). GS-0976 inhibited the accumulation of fat droplets and inflammatory cell infiltration (Figs. 2C–2F, 2N, 2O). The hepatic steatosis score ($P < 0.001$) and inflammation score ($P < 0.05$) were decreased by GS-0976 (Figs. 2P, 2Q). The Sirius Red staining results showed that the fibrosis area was decreased by GS-0976 in NASH (Figs. 2I–2L, 2R). The NAS score of the GS-0976 group (4.4 ± 0.245) was lower than that of the Model group (6.0 ± 0.0, $P < 0.05$) (Fig. 2S). These results showed that GS-0976 could inhibit the inflammation, fibrosis and hepatic steatosis in NASH.

RNA-Seq and DEG analysis

In order to study the global transcriptomic changes in gene expression induced by GS-0976 treatment in CDAHFD-induced NASH model, total RNA was extracted from the liver tissues of the Model group, GS-0976 group and Control group ($N = 3$) after eight weeks' GS-0976 or vehicle treatment. RNA-Seq was subsequently performed on the Illumina Hiseq platform. A total of 30,792,280, 28,201,679 and 31,217,825 raw reads were obtained from the three groups, respectively. Following quality control and the removal of duplicate, ambiguous and low-quality reads, a total of 29,878,505, 27,680,698, and 30,460,759 clean

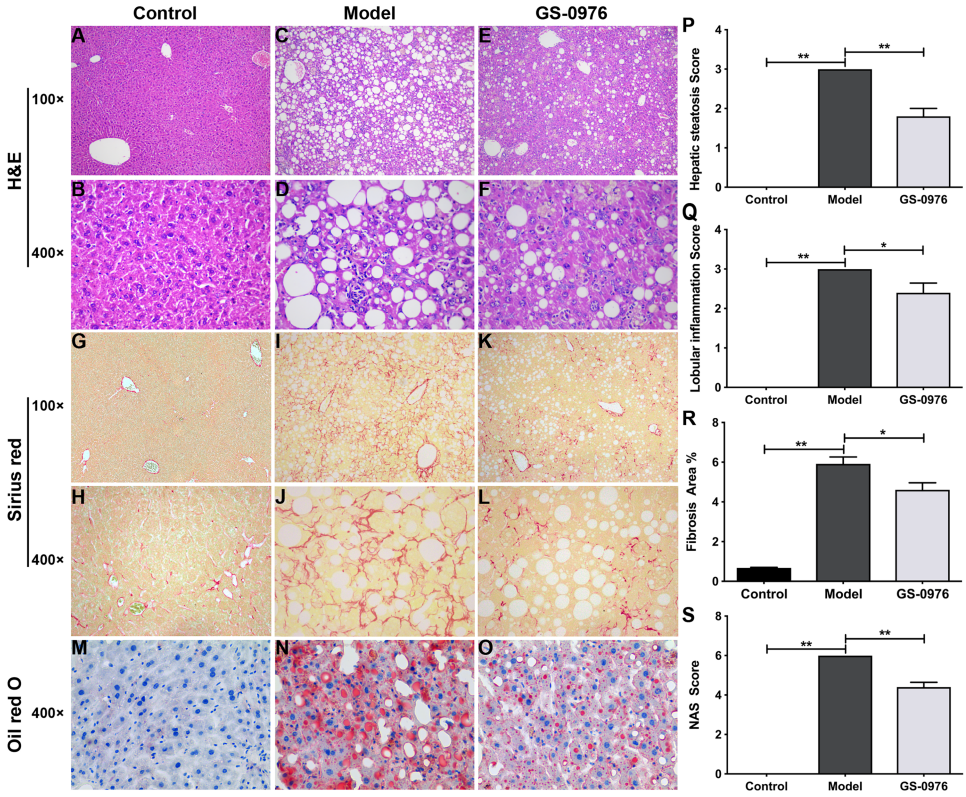

Figure 2 Effect of GS-0976 on liver histology in CDAHFD-induced NASH model. Histological evaluations of liver were performed in each group ($n = 5$). Paraffin-embedded liver sections were stained with H&E (A–F), Sirius red (G–L) and Oil Red O (M–O). Representative photographs of each group were presented. Images were obtained at 100× and 400×, respectively. Global hepatic steatosis (P), inflammation (Q), fibrosis (R), and NAS score (S) were analyzed in a blinded manner or by digital image analyzer. Data are shown as means ± SEM. $^{*}P < 0.05$, $^{**}P < 0.001$ compared with the Model group by one-way ANOVA with LSD test.

Full-size DOI: 10.7717/peerj.8115/fig-2

reads were attained from cDNA libraries respectively. Over 93% of the clean reads had a quality score equal or above Q30 level (sequencing error rate 0.01%), supporting the preciseness of sequencing. To identify genes significantly altered under GS-0976 exposure, DEGs analysis was executed with the DEGSeq R package (1.20.0) and the *P* values were adjusted by the Benjamin-Hochberg method. DEGs were identified as either up or down regulated with a P_{adj} threshold of 0.05 between treatment groups. And the results were displayed by volcano plots (Fig. 3A). The expression of 516 genes was up-regulated and 525 genes was down-regulated of 1,041 altered genes. The genes associated with NASH were selected and their expression profiles were analyzed by group comparisons (Fig. 3B). Quantitative RT-PCR was performed to validate the differential expression of representative genes. The results of qRT-PCR conformed the results of RNA-seq (Figs. 3C–3E). GS-0976 treatment inhibited the alterations of gene expression induced by CDAHFD feeding.

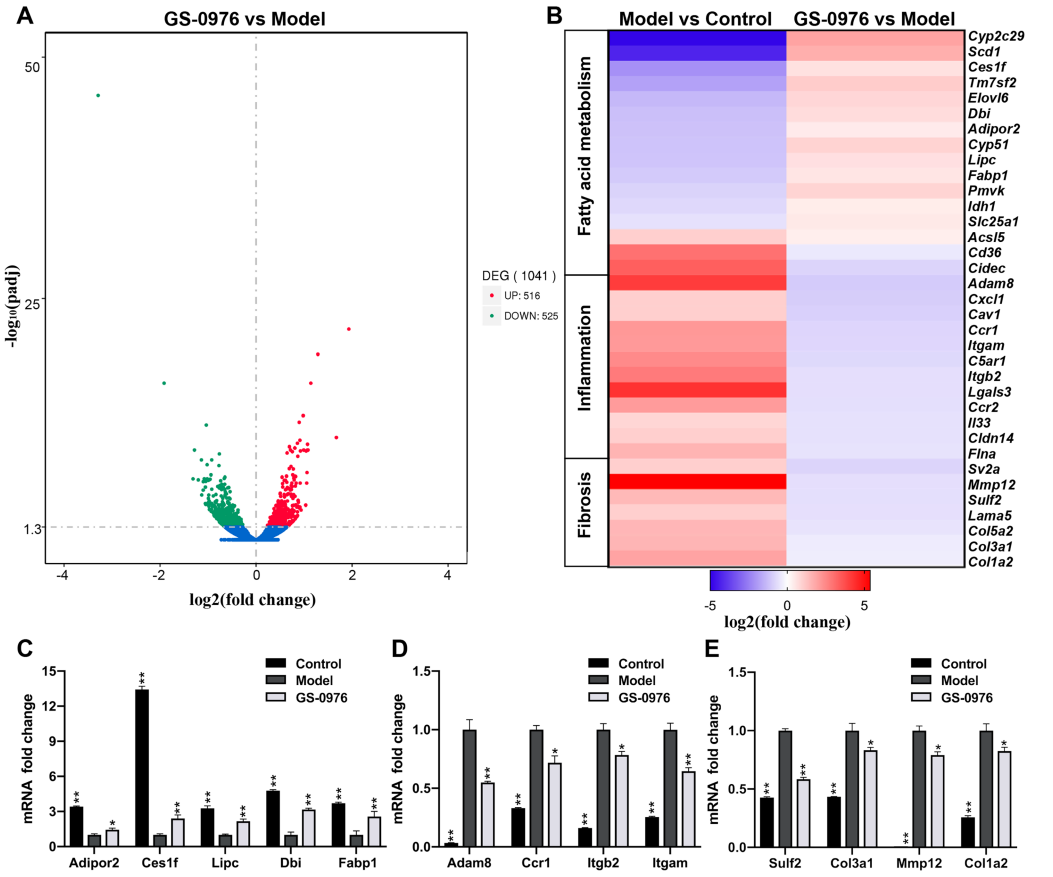

Figure 3 Global transcriptomic response and GS-0976-mediated signatures in NASH livers. (A) Global gene expression changes between the Model and the GS-0976 treatment group at mRNA level are shown in volcano plots of $\log_2$ (fold change) versus $-\log_{10}$ (P-value). Red dots indicate up-regulated DEGs, the green dots indicate down-regulated DEGs, and blue dots represent non-DEGs. (B) Heat map shows expression analysis of selected genes associated with fatty acid metabolism, inflammation and fibrosis. Color coded as $\log_2$ (fold change) from −5 to 5.4 with $P_{adj} < 0.05$. Quantitative RT-PCR was used to verify the differentially expressed genes related to fatty acid metabolism (C), inflammation (D) and fibrosis (E) identified by RNA-Seq analysis. Data are shown as means ± SEM; $n = 3$. $^{*}P < 0.05$, $^{**}P < 0.001$ compared with the Model group by one-way ANOVA with LSD test.

Full-size DOI: 10.7717/peerj.8115/fig-3

Bioinformatics analysis

To better understand the effect of GS-0976 on gene expression in the CDAHFD-induced NASH model, we performed GO analysis to categorize DEGs into relevant functions. In our study, 1041 DEGs were classified into 212 biological process (BP) terms, 25 cellular component (CC) terms, and 80 molecular function (MC) terms. Most of the enriched BP terms of up-regulated DEGs were categorized into metabolic processes. And the most significant BP terms of down-regulated DEGs were involved in extracellular matrix formation (GO: 0030198), wound healing (GO:0042060), cell chemotaxis (GO: 0060326), leukocyte migration (GO: 0050900) and angiogenesis (GO:0001525). The top 20 significant GO-BP terms were shown in Figs. 4A and 4B.

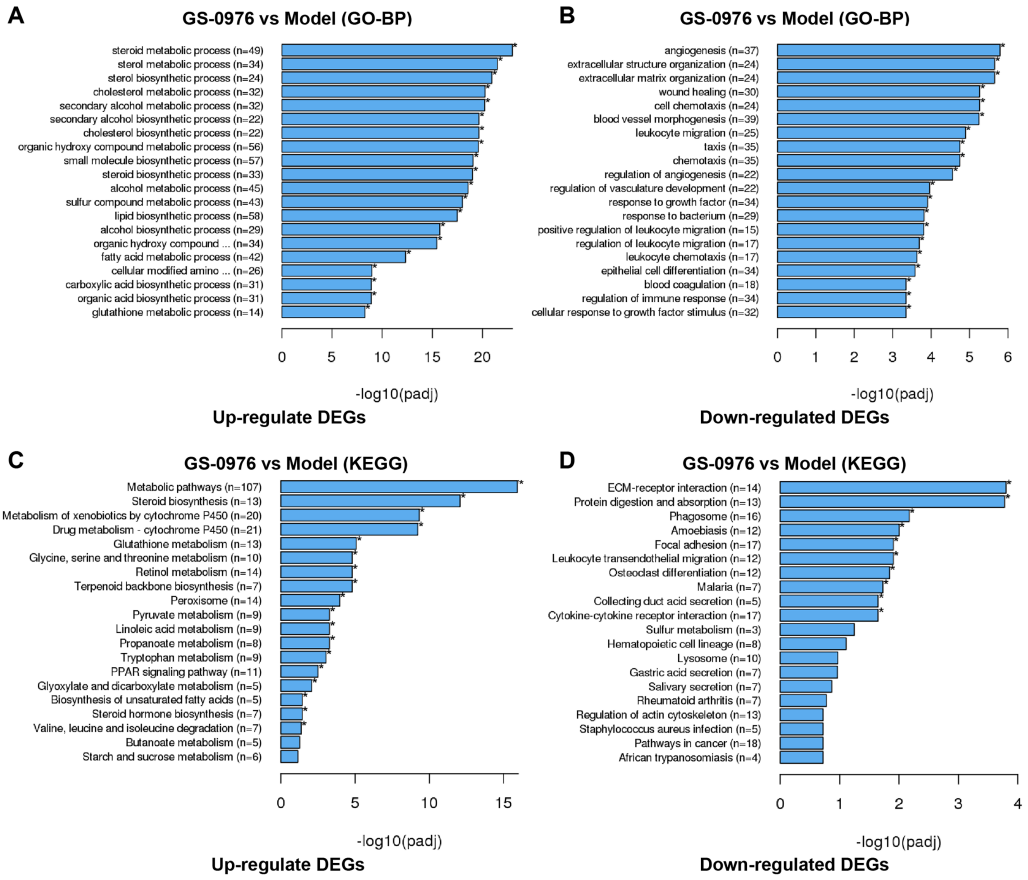

Figure 4 GO and KEGG enrichment analysis of DEGs. Top 20 GO biological process categories of significantly up- (A) and down-regulated (B) DEGs were presented in bar charts. Top 20 KEGG pathways among the up- (C) or down-regulated (D) DEGs were presented in bar charts.

Full-size DOI: 10.7717/peerj.8115/fig-4

To further identify relevant biological pathways, KEGG pathway analysis were performed based on the annotation results. The top 20 KEGG pathways among the up- or down-regulated DEGs were showed in Figs. 4C and 4D. The most significantly enriched pathway was "Metabolic pathways" including 107 up-regulated DEGs. As for the down-regulated DEGs, enriched pathways included "ECM-receptor interaction", "Protein digestion and absorption", "Leukocyte transendothelial migration", "Focal adhesion" and "Cytokine-cytokine receptor interaction". Some of the pathways and the corresponding genes were mapped by Pathview (Fig. 5) and listed in Table 1.

In vitro validation of GS-0976 on lipid accumulation and fibrosis

To further validated the effect of GS-0976 on lipid accumulation, the Oil red O staining was used to detect the lipid accumulation in FFA-induced LO2 cells treated with GS-0976. As shown in Figs. 6A–6E, the lipid accumulation was decreased by GS-0976 treatment at all dosages. The effect on anti-fibrosis is an important factor for evaluating the efficacy of drugs in NASH. Thus, the effects of GS-0976 on fibrosis were assessed in LX-2 cells. The mRNA levels of α-SMA, COL1A1, CTGF were significantly increased with 10 ng/mL

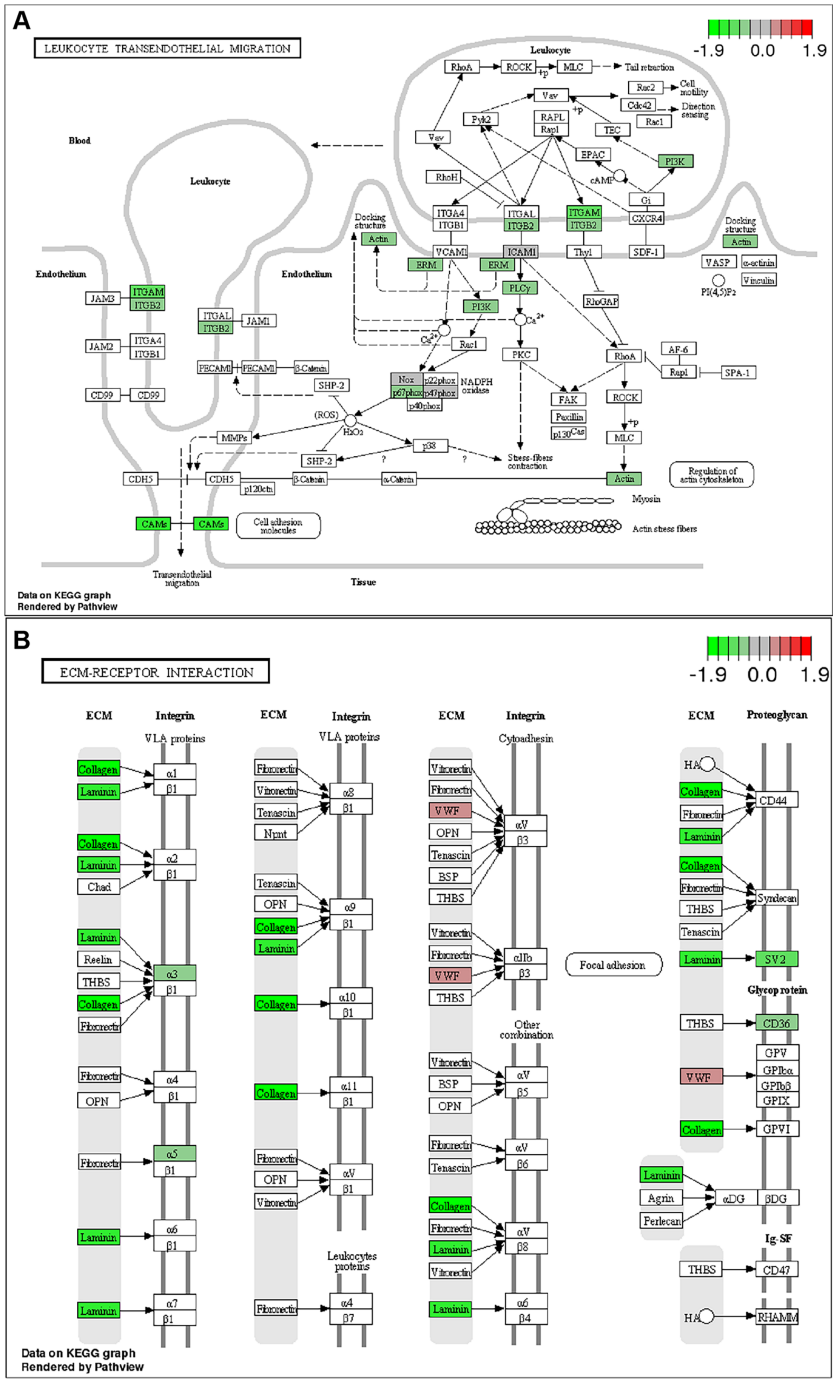

Figure 5 **KEGG pathway analysis .** List of the DEGs implicated in "Leukocyte transendothelial migration" (A) and "ECM-receptor interaction" (B) signaling pathways. The red frames represent upregulated DEGs; the green frames represent downregulated DEGs .

Full-size DOI: 10.7717/peerj.8115/fig-5

Table 1 Lists of the representative different-expressed pathways and the corresponding affected genes.

Description	BgRatio	P_{adj}	Gene ID
Metabolic pathways	1106/5208	1.16E−16	Cyp2c29/Idi1/Pmvk/Tm7sf2/Gclc/Sqle/Rdh11/Nsdhl/Cyp51/Hmgcs1/Ugdh/Acss2/ Acat2/Msmo1/Me1/Fdft1/Cbs/Qdpr/Sc5d/ Ebp/Acacb/Lipc/Kynu/Lss/Mvd/Acaca/Adh4/Mvk/Coasy/Ddc/Dhcr7/Cyp2c38/ Cyp27a1/Pi4k2b/Aox1/Cyp2j5/Cyp2r1/Aldh1a7/Cyp2c55/Cyp4f14/ Cyp1a2/Tat/Haao/9130409I23Rik/ Cyp3a11/Hibadh/Gldc/Ugt2b36/Sgms2/Pcyt2/Ugt2b5/Idh1/Fdps/ Gbe1/Ndufa4/Csad/Mmab/Comt/Atp5j/Acmsd/Agxt/Cyp2c44/Mdh1/Dhcr24/ Cat/Paics/St3gal3/Slc33a1/Tgds/Scp2/Aldh7a1/Oat/ Akr1c6/Adk/Hsd17b7/Amt/Amdhd1/Pcca/Pon1/Hsd17b2/Acsl5/Ndufv3/Mcee/Hyi/ Lap3/Mat2b/Baat/Enpp3/Cyp2c70/Btd/Adi1/ Cept1/Atp5g1/Gclm/Pik3c3/Cbr3/Gatm/Pipox/ Cox6c/Acly/Otc/Nat2/Glud1/Acss3/Khk/Acsm5/Atp5e
ECM-receptor interaction	84/5208	0.00015843	Cd36/Itga5/Col5a2/Col4a4/Lama5/Sv2a/Col6a1/Lamb2/Col3a1/Col4a1/ Col1a2/Col4a6/Col6a2/Itga3
Protein digestion and absorption	77/5208	0.00016717	Atp1a3/Kcnn4/Col5a2/Col4a4/Slc1a5/Col6a1/Col3a1/Col4a1/Slc7a8/ Col1a2/Col14a1/Col4a6/Col6a2
Leukocyte transendothelial migration	111/5208	0.01246479	Itgb2/Itgam/Cldn14/Cldn15/Actg1/Ezr/Plcg2/Icam1/Pik3r5/Cybb/Ncf1/Ncf2
Focal adhesion	196/5208	0.01246479	Flna/Cav1/Itga5/Col5a2/Col4a4/Lama5/Actg1/Col6a1/Tln1/Lamb2/Col3a1/ Col4a1/Col1a2/Col4a6/Pik3r5/Col6a2/Itga3
Cytokine-cytokine receptor interaction	216/5208	0.02264483	Cxcl1/Ccr1/Csf2rb/Csf2ra/Ccr2/Tnfrsf12a/Inhbe/Lepr/Tnfrsf1b/Kitl/ Clcf1/Pf4/Ccl6/Il6ra/Csf1r/Cxcl14/Tnfrsf11b

TGF- β1 stimulation and these changes were inhibited by GS-0976 (Fig. 6F). Besides, the decreased expression of *COL1A2*, *COL3A1*, *SULF2* found in vivo were observed in TGF-β1-induced LX-2 cells with GS-0976 treatment (Fig. 6F).

DISCUSSION

In this study, we confirmed the effect of GS-0976 in CDAHFD-induced NASH model. RNA-Seq transcriptome was used to analyze the gene expression profiles in mice treated with GS-0976. Functional enrichment analysis of the DEGs highlighted the pathways involved in metabolic, fibrosis and immune/ inflammation processes.

Various NASH mouse models have been established based on different genetic or dietary operations (*Santhekadur, Kumar & Sanyal, 2018*). And there was no universal mouse model of NASH for not well-replicating human disease or rapidly progressing to fibrosis. In our study, the CDAHFD consisting of 60% kcal fat and 0.1% methionine was used to establish NASH model in C57BL/6 mice. Studies have reported that mice fed with CDAHFD showed excessive fat accumulation in the liver and rapidly developed progressive hepatic fibrosis with the body weight mildly changed. Thus, CDAHFD-induced NASH model can be potentially useful for understanding human NASH (*Jain et al., 2018*; *Matsumoto et al., 2013*; *Susutlertpanya et al., 2019*).

Studies have showed that hepatic steatosis is the primary cause for NAFLD/NASH. The accumulation of lipid will lead to cell damage, organelle dysfunction, and chronic inflammation. Saturated fatty acids (SFA), including palmitate acid and stearate acid, have

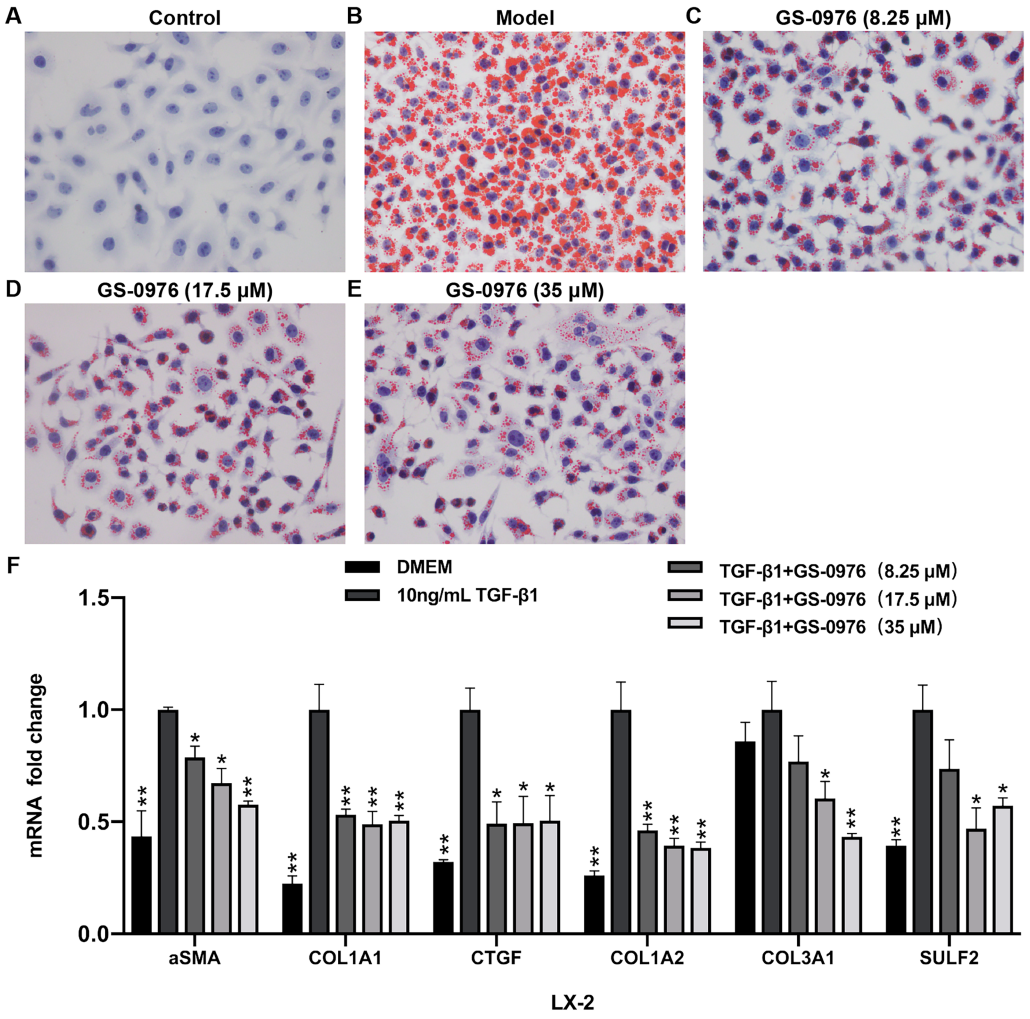

Figure 6 GS-0976 reduced lipid accumulation and expression of profibrogenic genes. (A–E) Oil Red O staining was performed in LO2 cells after treatment with the indicated GS-0976 in the presence of 0.8 mM FFA for 24 h. Original magnification , 400 ×. (F) Quantitative RT-PCR assessments of the mRNA levels of α-SMA, COL1A1, CTGF , COL1A2, COL3A1, SULF2 in response to GS-0976 treatment in LX-2 cells. Data are presented as means ±SEM; $n = 3$. $^{*}P < 0.05$, $^{**}P < 0.001$ compared with the 10 ng/mL TGF- β1 treatment group by One-way ANOVA with LSD test.

Full-size DOI: 10.7717/peerj.8115/fig-6

lipotoxicity in the steatotic liver (*Musso et al., 2018*). There are two ways to inhibit hepatic SFA lipotoxicity. One is to regulate nuclear transcription factors through LXR-α (liver X receptor α), FXR (farnesoid X receptor) and peroxisome proliferator–activated receptors (PPARs). The other is to inhibit the enzymes involved in lipid synthesis (*Musso et al., 2018*). Inhibition of Acetyl-CoA carboxylase, the first rate-limiting enzymes involved in de novo fatty acid synthesis, is an effective way to inhibit lipotoxicity. The previous study has showed that NASH patients received GS-0976 20 mg daily for 12 weeks, hepatic lipid was decreased (*Lawitz et al., 2018*). In our study, the hepatic steatosis was decreased by GS-0976 treatment in CDAHFD-induced NASH model (Figs. 2C–2F, 2N, 2O). These results were confirmed

in vitro hepatic steatosis cell model (Figs. 6A–6E). The underlying mechanism of GS-0976 in decreasing hepatic steatosis was indicated by RNA-Seq transcriptome analysis. GS-0976 regulated the genes associated with metabolic pathways. These genes involved in fatty acid oxidation were significantly increased, such as *Dbi* and *Fabp1*, encoding the binding protein of acyl-CoA and free fatty acid for mitochondrial β-oxidation. FABP1 expression was shown to be overexpressed in simple steatosis, but underexpressed in NASH patients. The decrease of FABP1 expression could inhibit its detergent effect on FFA (*Charlton et al., 2009*). Lipid catabolic genes such as *Ces1f* and *Lipc* were up-regulated. Adiponectin receptor 2 (*AdipoR 2*) involved in the PPAR α pathway activation was up-regulated as well (*Kadowaki & Yamauchi, 2005*) (Figs. 3B, 3C). However, the up-regulation of several genes involved in steroid, cholesterol and fatty acid biosynthesis were observed with GS-0976 treatment, such as stearoyl-CoA desaturase 1 (*Scd1*), Phosphomevalonate kinase (Pmvk) and elongation of long-chain fatty acids family member 6 (*Elovl6*). These genes were down-regulated with CDAHFD feeding (Fig. 3B). The homeostasis and compensatory response of liver might explain these results. Ye et al. reported that *Hmgcr,* encoding the rate-limiting enzyme in cholesterol biosynthesis, was down-regulated with high-fat diet plus streptozocin feeding (*Ye et al., 2016*). It was possible for liver to maintain homeostasis in response to CDAHFD thus resulted in the down-regulation of these genes. Besides, studies indicated that ACC deficiency directly led to a reduction of malonyl-CoA and further repressed the endogenous synthesis of polyunsaturated fatty acids (PUFAs), which in turn could result in the activation of *Srebp-1c* (*Kim et al., 2017*). SREBP-1c is a transcription factor that largely regulates the genes involved in fatty acid synthesis including *Scd1* and *Elovl6* (*Horton, Goldstein & Brown, 2002*).

Chronic liver inflammation promotes the development of NASH and fibrosis (*Farrell & Larter, 2006*). In this study, the CDAHFD feeding induced liver inflammatory cell infiltration. Studies showed ND-654, the analog of GS-0976, reduced neutrophil recruitment by decreasing the pro-inflammatory cytokines including Cxcl1 on a chronic inflammation HCC model (*Lally et al., 2019*). Here we reported the effect of ACC inhibition in NASH-related inflammation. Although GS-0976 treatment modestly alleviated inflammation by H&E staining (Figs. 2C–2F), RNA-Seq analysis showed that the enriched DEGs and pathways were significantly involved in in inflammatory process. Genes of integrin (*Itgam/Itgb2*), claudin (*Cldn14/Cldn15*), chemokine (*Cxcl1/Ccr1/Ccr2*), filamin (*Flna*) and caveolin (*Cav1*) are involved in "Leukocyte activation and migration", "Cytokine-cytokine receptor interaction" and "Focal adhesion" pathways. The expressions of these genes were significantly down-regulated by GS-0976 treatment (Figs. 3B, 3D; Table 1). Thus, GS-0976 treatment attenuated inflammation in CDAHFD-induced NASH model.

Hepatic fibrosis can promote the development of NASH and is associated with poor clinical outcomes in NASH. Anti-fibrotic effects of ACC inhibitor have been noticed by several studies. The serum fibrosis marker TIMP1 was decreased both in a proof-of-concept study and the phase II trial of NASH patients treated with GS-0976 (*Lawitz et al., 2018*; *Loomba et al., 2018*). The beneficial effects in rat fibrosis models and primary hepatic stellate cells of GS-834356, an analog of GS-0976, were reported (*Bates et al., 2018*). The anti-fibrosis mechanism of GS-0976 has not been fully elucidated. In this study, Sirius red

showed that GS-0976 could significantly reduce the fibrosis in the CDAHFD NASH model (Figs. 2I–2L). According to the RNA-Seq analysis, GS-0976 downregulated genes related to ECM function and structure, including ECM receptor interaction, protein digestion and absorption, local adhesion and extracellular matrix organization (Table 1). Moreover, GS-0976 can inhibit the expressions of α-SMA, *COL1A1*, *CTGF*, *COL1A2*, *COL3A1*, *SULF2* in LX-2 cells, suggesting that GS-0976 has a direct anti-fibrotic effect (Fig. 6F).

It has been reported that NASH is accompanied by increased angiogenesis both in human and animal experimental models (*Kitade et al., 2006*; *Kitade et al., 2008*). Increased angiogenesis can promote the inflammation and fibrosis in NASH. Studies have demonstrated that the inhibition of angiogenic response by suppressing the interaction between VEGF signaling and Ang-2/Tie2 attenuated the severity of NASH in experimental models (*Coulon et al., 2013*; *Lefere et al., 2019*). In our study, the GO terms of angiogenesis and blood vessel morphogenesis were significantly enriched in down-regulated DEGs (Fig. 4B), suggesting the potential efficiency of GS-0976 on angiogenesis.

CONCLUSION

GS-0976 attenuated liver injury in CDAHFD-induced NASH model. Comparative RNA-seq transcriptome analysis showed that GS-0976 can regulate the expression of genes involved in the metabolism, inflammation, fibrosis and angiogenesis of NASH. These results further elucidate the mechanisms of GS-0976 in NASH.

ACKNOWLEDGEMENTS

The authors thank the research platform provided by Public Health and Preventive Medicine Provincial Experiment Teaching Center at Sichuan University and Food Safety Monitoring and Risk Assessment Key Laboratory of Sichuan Province.

ADDITIONAL INFORMATION AND DECLARATIONS

Funding

This work was supported by the National Natural Science Foundation of China (No. 81773375 and 81802801) and the National Science and Technology Major Project "Key New Drug Creation and Manufacturing Program", China (NO. 2019ZX09201001). The funders had no role in study design, data collection and analysis, decision to publish, or preparation of the manuscript.

Grant Disclosures

The following grant information was disclosed by the authors:
National Natural Science Foundation of China: No. 81773375 and 81802801.
National Science and Technology Major Project "Key New Drug Creation and Manufacturing Program", China: 2019ZX09201001.

Competing Interests

The authors declare there are no competing interests. Qianru Zhang is an employee of Guangdong Zhongsheng Pharmaceutical Co., Ltd. Jinliang Yang and Yuqin Yao are cooperative partners and academic consultants of Guangdong Zhongsheng Pharmaceutical Co., Ltd.

Author Contributions

- Ying Lu performed the experiments, analyzed the data, prepared figures and/or tables, authored or reviewed drafts of the paper, approved the final draft.
- Xiaolan Su and Qianru Zhang performed the experiments, analyzed the data, prepared figures and/or tables, approved the final draft.
- Manyu Zhao performed the experiments, analyzed the data, authored or reviewed drafts of the paper, approved the final draft.
- Chuang Liu performed the experiments, prepared figures and/or tables, approved the final draft.
- Qinhuai Lai and Sijia Wu analyzed the data, contributed reagents/materials/analysis tools, prepared figures and/or tables, approved the final draft.
- Aiping Fang analyzed the data, contributed reagents/materials/analysis tools, authored or reviewed drafts of the paper, approved the final draft.
- Jinliang Yang, Xiaoxin Chen and Yuqin Yao conceived and designed the experiments, authored or reviewed drafts of the paper, approved the final draft.

Animal Ethics

The following information was supplied relating to ethical approvals (i.e., approving body and any reference numbers):

West China Hospital, Sichuan University approved the animal experiments (approval no.182).

Data Availability

The following information was supplied regarding data availability:

The raw data is available in the Supplemental Files.

Supplemental Information

Supplemental information for this article can be found online at http://dx.doi.org/10.7717/peerj.8115#supplemental-information.

REFERENCES

Abu-Elheiga L, Jayakumar A, Baldini A, Chirala SS, Wakil SJ. 1995. Human acetyl-CoA carboxylase: characterization, molecular cloning, and evidence for two isoforms. *Proceedings of the National Academy of Sciences of the United States of America* **92**:4011–4015 DOI 10.1073/pnas.92.9.4011.

Bates J, Ghoshal S, Wei L, Hollenback D, Liu K, Kusam S, Sulfab M, Liu H, Brockett R, Newstrom D, Mikaelian I, Wang T, Harriman G, Westlin WF, Rocnik J,

Harwood HJ, Kapeller R, Ray A, Breckenridge D, Fuchs BC. 2018. ACC inhibitor demonstrates potent anti-fibrotic activity in vitro and in vivo. *Journal of Hepatology* **68**:S399–S400 DOI 10.1016/s0168-8278(18)31036-5.

Bedossa P. 2017. Pathology of non-alcoholic fatty liver disease. *Liver International* **37(Suppl 1)**:85–89 DOI 10.1111/liv.13301.

Chalasani N, Younossi Z, Lavine JE, Charlton M, Cusi K, Rinella M, Harrison SA, Brunt EM, Sanyal AJ. 2018. The diagnosis and management of nonalcoholic fatty liver disease: practice guidance from the American Association for the Study of Liver Diseases. *Hepatology* **67**:328–357 DOI 10.1002/hep.29367.

Charlton M, Viker K, Krishnan A, Sanderson S, Veldt B, Kaalsbeek AJ, Kendrick M, Thompson G, Que F, Swain J, Sarr M. 2009. Differential expression of lumican and fatty acid binding protein-1: new insights into the histologic spectrum of nonalcoholic fatty liver disease. *Hepatology* **49**:1375–1384 DOI 10.1002/hep.22927.

Chen J, Yao Y, Su X, Shi Y, Song X, Xie L, You J, Tian L, Yang L, Fang A, Xiong J. 2018. Comparative RNA-Seq transcriptome analysis on silica induced pulmonary inflammation and fibrosis in mice silicosis model. *Journal of Applied Toxicology* **38**:773–782 DOI 10.1002/jat.3587.

Coulon S, Legry V, Heindryckx F, Van Steenkiste C, Casteleyn C, Olievier K, Libbrecht L, Carmeliet P, Jonckx B, Stassen JM, Van Vlierberghe H, Leclercq I, Colle I, Geerts A. 2013. Role of vascular endothelial growth factor in the pathophysiology of nonalcoholic steatohepatitis in two rodent models. *Hepatology* **57**:1793–1805 DOI 10.1002/hep.26219.

Estes C, Razavi H, Loomba R, Younossi Z, Sanyal AJ. 2018. Modeling the epidemic of nonalcoholic fatty liver disease demonstrates an exponential increase in burden of disease. *Hepatology* **67**:123–133 DOI 10.1002/hep.29466.

Farrell GC, Larter CZ. 2006. Nonalcoholic fatty liver disease: from steatosis to cirrhosis. *Hepatology* **43**:S99–S112 DOI 10.1002/hep.20973.

Harriman G, Greenwood J, Bhat S, Huang X, Wang R, Paul D, Tong L, Saha AK, Westlin WF, Kapeller R, Harwood Jr HJ. 2016. Acetyl-CoA carboxylase inhibition by ND-630 reduces hepatic steatosis, improves insulin sensitivity, and modulates dyslipidemia in rats. *Proceedings of the National Academy of Sciences of the United States of America* **113**:E1796–E1805 DOI 10.1073/pnas.1520686113.

Harwood Jr HJ, Petras SF, Shelly LD, Zaccaro LM, Perry DA, Makowski MR, Hargrove DM, Martin KA, Tracey WR, Chapman JG, Magee WP, Dalvie DK, Soliman VF, Martin WH, Mularski CJ, Eisenbeis SA. 2003. Isozyme-nonselective N-substituted bipiperidylcarboxamide acetyl-CoA carboxylase inhibitors reduce tissue malonyl-CoA concentrations, inhibit fatty acid synthesis, and increase fatty acid oxidation in cultured cells and in experimental animals. *Journal of Biological Chemistry* **278**:37099–37111 DOI 10.1074/jbc.M304481200.

Horton JD, Goldstein JL, Brown MS. 2002. SREBPs: activators of the complete program of cholesterol and fatty acid synthesis in the liver. *Journal of Clinical Investigation* **109**:1125–1131 DOI 10.1172/jci0215593.

Jain MR, Giri SR, Bhoi B, Trivedi C, Rath A, Rathod R, Ranvir R, Kadam S, Patel H, Swain P, Roy SS, Das N, Karmakar E, Wahli W, Patel PR. 2018. Dual PPARalpha/gamma agonist saroglitazar improves liver histopathology and biochemistry in experimental NASH models. *Liver International* **38**:1084–1094 DOI 10.1111/liv.13634.

Kadowaki T, Yamauchi T. 2005. Adiponectin and adiponectin receptors. *Endocrine Reviews* **26**:439–451 DOI 10.1210/er.2005-0005.

Kim CW, Addy C, Kusunoki J, Anderson NN, Deja S, Fu X, Burgess SC, Li C, Ruddy M, Chakravarthy M, Previs S, Milstein S, Fitzgerald K, Kelley DE, Horton JD. 2017. Acetyl CoA carboxylase inhibition reduces hepatic steatosis but elevates plasma triglycerides in mice and humans: a bedside to bench investigation. *Cell Metabolism* **26**:394–406 DOI 10.1016/j.cmet.2017.07.009.

Kitade M, Yoshiji H, Kojima H, Ikenaka Y, Noguchi R, Kaji K, Yoshii J, Yanase K, Namisaki T, Asada K, Yamazaki M, Tsujimoto T, Akahane T, Uemura M, Fukui H. 2006. Leptin-mediated neovascularization is a prerequisite for progression of nonalcoholic steatohepatitis in rats. *Hepatology* **44**:983–991 DOI 10.1002/hep.21338.

Kitade M, Yoshiji H, Kojima H, Ikenaka Y, Noguchi R, Kaji K, Yoshii J, Yanase K, Namisaki T, Yamazaki M, Tsujimoto T, Moriya K, Kawaratani H, Akahane T, Fukui H. 2008. Neovascularization and oxidative stress in the progression of non-alcoholic steatohepatitis. *Molecular Medicine Reports* **1(4)**:543–548 DOI 10.3892/mmr.1.4.543.

Kleiner DE, Brunt EM, Van Natta M, Behling C, Contos MJ, Cummings OW, Ferrell LD, Liu YC, Torbenson MS, Unalp-Arida A, Yeh M, McCullough AJ, Sanyal AJ, Nonalcoholic Steatohepatitis Clinical Research Network. 2005. Design and validation of a histological scoring system for nonalcoholic fatty liver disease. *Hepatology* **41**:1313–1321 DOI 10.1002/hep.20701.

Lai Q, Wang Y, Wang R, Lai W, Tang L, Tao Y, Liu Y, Zhang R, Huang L, Xiang H, Zeng S, Gou L, Chen H, Yao Y, Yang J. 2018. Design, synthesis and biological evaluation of a novel tubulin inhibitor 7a3 targeting the colchicine binding site. *European Journal of Medicinal Chemistry* **156**:162–179 DOI 10.1016/j.ejmech.2018.05.010.

Lally JSV, Ghoshal S, DePeralta DK, Moaven O, Wei L, Masia R, Erstad DJ, Fujiwara N, Leong V, Houde VP, Anagnostopoulos AE, Wang A, Broadfield LA, Ford RJ, Foster RA, Bates J, Sun H, Wang T, Liu H, Ray AS, Saha AK, Greenwood J, Bhat S, Harriman G, Miao W, Rocnik JL, Westlin WF, Muti P, Tsakiridis T, Harwood Jr HJ, Kapeller R, Hoshida Y, Tanabe KK, Steinberg GR, Fuchs BC. 2019. Inhibition of Acetyl-CoA Carboxylase by phosphorylation or the inhibitor ND-654 suppresses lipogenesis and hepatocellular carcinoma. *Cell Metabolism* **29**:174–182 DOI 10.1016/j.cmet.2018.08.020.

Lawitz EJ, Coste A, Poordad F, Alkhouri N, Loo N, McColgan BJ, Tarrant JM, Nguyen T, Han L, Chung C, Ray AS, McHutchison JG, Subramanian GM, Myers RP, Middleton MS, Sirlin C, Loomba R, Nyangau E, Fitch M, Li K, Hellerstein M. 2018. Acetyl-CoA carboxylase inhibitor GS-0976 for 12 weeks reduces hepatic De

Novo Lipogenesis and steatosis in patients with nonalcoholic steatohepatitis. *Clinical Gastroenterology and Hepatology* **16(12)**:1983–1991 DOI 10.1016/j.cgh.2018.04.042.

Lefere S, Van de Velde F, Hoorens A, Raevens S, Van Campenhout S, Vandierendonck A, Neyt S, Vandeghinste B, Vanhove C, Debbaut C, Verhelst X, Van Dorpe J, Van Steenkiste C, Casteleyn C, Lapauw B, Van Vlierberghe H, Geerts A, Devisscher L. 2019. Angiopoietin-2 promotes pathological angiogenesis and is a therapeutic target in murine nonalcoholic fatty liver disease. *Hepatology* **69**:1087–1104 DOI 10.1002/hep.30294.

Loomba R, Kayali Z, Noureddin M, Ruane P, Lawitz EJ, Bennett M, Wang L, Harting E, Tarrant JM, McColgan BJ, Chung C, Ray AS, Subramanian GM, Myers RP, Middleton MS, Lai M, Charlton M, Harrison SA. 2018. GS-0976 reduces hepatic steatosis and fibrosis markers in patients with nonalcoholic fatty liver disease. *Gastroenterology* **155**:1463–1473 DOI 10.1053/j.gastro.2018.07.027.

Mao J, DeMayo FJ, Li H, Abu-Elheiga L, Gu Z, Shaikenov TE, Kordari P, Chirala SS, Heird WC, Wakil SJ. 2006. Liver-specific deletion of acetyl-CoA carboxylase 1 reduces hepatic triglyceride accumulation without affecting glucose homeostasis. *Proceedings of the National Academy of Sciences of the United States of America* **103**:8552–8557 DOI 10.1073/pnas.0603115103.

Matsumoto M, Hada N, Sakamaki Y, Uno A, Shiga T, Tanaka C, Ito T, Katsume A, Sudoh M. 2013. An improved mouse model that rapidly develops fibrosis in non-alcoholic steatohepatitis. *International Journal of Experimental Pathology* **94**:93–103 DOI 10.1111/iep.12008.

Musso G, Cassader M, Paschetta E, Gambino R. 2018. Bioactive lipid species and metabolic pathways in progression and resolution of nonalcoholic steatohepatitis. *Gastroenterology* **155**:282–302 DOI 10.1053/j.gastro.2018.06.031.

Neuschwander-Tetri BA. 2010. Hepatic lipotoxicity and the pathogenesis of nonalcoholic steatohepatitis: the central role of nontriglyceride fatty acid metabolites. *Hepatology* **52**:774–788 DOI 10.1002/hep.23719.

Santhekadur PK, Kumar DP, Sanyal AJ. 2018. Preclinical models of non-alcoholic fatty liver disease. *Journal of Hepatology* **68**:230–237 DOI 10.1016/j.jhep.2017.10.031.

Susutlertpanya W, Wakuda H, Otani N, Kuramoto T, Li L, Kuranari M, Sekiguchi A, Kudo H, Uchida T, Imai H, Uemura N. 2019. Histological evaluation of nintedanib in non-alcoholic steatohepatitis mice. *Life Sciences* **228**:251–257 DOI 10.1016/j.lfs.2019.05.014.

Ye JH, Chao J, Chang ML, Peng WH, Cheng HY, Liao JW, Pao LH. 2016. Pentoxifylline ameliorates non-alcoholic fatty liver disease in hyperglycaemic and dyslipidaemic mice by upregulating fatty acid beta-oxidation. *Scientific Reports* **6**:33102 DOI 10.1038/srep33102.

Younossi Z, Anstee QM, Marietti M, Hardy T, Henry L, Eslam M, George J, Bugianesi E. 2018a. Global burden of NAFLD and NASH: trends, predictions, risk factors and prevention. *Nature Reviews Gastroenterology & Hepatology* **15**:11–20 DOI 10.1038/nrgastro.2017.109.

Younossi ZM, Loomba R, Rinella ME, Bugianesi E, Marchesini G, Neuschwander-Tetri BA, Serfaty L, Negro F, Caldwell SH, Ratziu V, Corey KE, Friedman SL, Abdelmalek MF, Harrison SA, Sanyal AJ, Lavine JE, Mathurin P, Charlton MR, Chalasani NP, Anstee QM, Kowdley KV, George J, Goodman ZD, Lindor K. 2018b. Current and future therapeutic regimens for nonalcoholic fatty liver disease and nonalcoholic steatohepatitis. *Hepatology* **68**:361–371 DOI 10.1002/hep.29724.

Zhang H, Wang Y, Wu Y, Jiang X, Tao Y, Yao Y, Peng Y, Chen X, Fu Y, Yu L, Wang R, Lai Q, Lai W, Li W, Kang Y, Yi S, Lu Y, Gou L, Wu M, Yang J. 2017. Therapeutic potential of an anti-HER2 single chain antibody-DM1 conjugates for the treatment of HER2-positive cancer. *Signal Transduction and Targeted Therapy* **2**:Article 17015 DOI 10.1038/sigtrans.2017.15.